JACS
JOURNAL OF THE AMERICAN CHEMICAL SOCIETY
Article
pubs.acs.org/JACS

Selective Reduction of CO_2 to CH_4 by Tandem Hydrosilylation with Mixed Al/B Catalysts

Jiawei Chen,[†] Laura Falivene,*[,‡] Lucia Caporaso,[§] Luigi Cavallo,[‡] and Eugene Y.-X. Chen*[,†]

[†]Department of Chemistry, Colorado State University, Fort Collins, Colorado 80523-1872, United States

[‡]Physical Sciences and Engineering Division, Kaust Catalysis Center (KCC), King Abdullah University of Science and Technology (KAUST), Thuwal 23955-6900, Saudi Arabia

[§]Dipartimento di Chimica e Biologia, Università di Salerno, Via Papa Paolo Giovanni II, I-84084 Fisciano, Italy

Supporting Information

ABSTRACT: This contribution reports the first example of highly selective reduction of CO_2 into CH_4 via tandem hydrosilylation with mixed main-group organo-Lewis acid (LA) catalysts $[Al(C_6F_5)_3 + B(C_6F_5)_3]$ {[Al] + [B]}. As shown by this comprehensive experimental and computational study, in this unique tandem catalytic process, [Al] effectively mediates the first step of the overall reduction cycle, namely the fixation of CO_2 into $HCOOSiEt_3$ (**1**) via the LA-mediated C═O activation, while [B] is incapable of promoting the same transformation. On the other hand, [B] is shown to be an excellent catalyst for the subsequent reduction steps 2−4, namely the hydrosilylation of the more basic intermediates [**1** to $H_2C(OSiEt_3)_2$ (**2**) to $H_3COSiEt_3$ (**3**) and finally to CH_4] through the frustrated Lewis pair (FLP)-type Si−H activation. Hence, with the required combination of [Al] and [B], a highly selective hydrosilylative reduction of CO_2 system has been developed, achieving high CH_4 production yield up to 94%. The remarkably different catalytic behaviors between [Al] and [B] are attributed to the higher overall Lewis acidity of [Al] derived from two conflicting factors (electronic and steric effects), which renders the higher tendency of [Al] to form stable [Al]−substrate (intermediate) adducts with CO_2 as well as subsequent intermediates **1**, **2**, and **3**. Overall, the roles of [Al] and [B] are not only complementary but also synergistic in the total reduction of CO_2, which render both [Al]-mediated first reduction step and [B]-mediated subsequent steps catalytic.

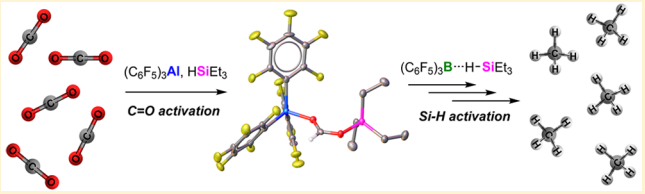

INTRODUCTION

Achieving efficient direct and catalytic reduction of CO_2 into CH_4 will have significant impact on addressing two currently biggest issues facing humanity: global warming largely due to the rising level of the greenhouse gas CO_2 and increasing demand on clean energy such as solar energy and natural gas CH_4. Although CO_2 is considered to be an ideal renewable C_1 feedstock for chemicals, materials, and fuels as it is renewable, abundant, nonflammable, and inexpensive,[1] it is a highly stable, inert molecule, so it has been a challenge to develop technologically feasible and economically competitive methods to convert CO_2 into fuels, especially high-energy density, deoxygenated fuels such as methane.[2] Catalytic hydrosilylation of CO_2, although with silanes as an expensive hydrogen source, is a thermodynamically favored process with formation of stronger Si−O bonds,[3] when compared to the catalytic hydrogenation of CO_2.[4] Currently, transition-metal (TM) catalysts based on metals such as Ru,[5] Co,[6] Rh,[7] Ir,[8] Ni,[9] Cu,[10] and main-group Zn[11] have been utilized but achieved limited success in the catalytic hydrosilylation of CO_2 to lower oxidation state species with low selectivity for methane formation.[2]

An emerging approach to enhancing catalytic performance of the CO_2 hydrosilylation systems is to couple the strong organo-Lewis acid $B(C_6F_5)_3$,[12] which, when used alone, is incapable of reducing CO_2,[13] with TM complexes of Zr,[13] Pt, Pd,[14] Re,[15] and Sc[16] for fixation of CO_2 (by TM complexes) and subsequent reduction of the more basic formate, aldehyde, and methanol equivalents to CH_4 (by the borane). More recently, there is emerging interest in the development of TM-free catalysis spotlighted by frustrated Lewis pairs (FLPs).[17] O'Hare et al. reported CO_2 can be hydrogenated to CH_3OH with the 2,2,6,6-tetramethylpiperidine (TMP)/$B(C_6F_5)_3$ FLP system.[18] Alternatively, Stephan[19] et al. demonstrated the combination of $PMes_3/AlX_3$ (Mes = mesityl, X = Cl, Br) effects the reduction of CO_2 to CH_3OH with H_3NBH_3 as a hydrogen source. However, both of these transformations require a stoichiometric amount of the FLP reagents. In this regard, Fontaine et al. discovered an ambiphilic Lewis pair system with a less Lewis acidic catecholboryl unit which can promote the release of the reduced products from the catalyst and thus render the hydroboration of CO_2 catalytic.[20] Ever since, major experimental and computational efforts have been directed to the study of the CO_2 reduction utilizing the FLP chemistry.[21,22] On the other hand, only a few examples of catalytic hydrosilylation of CO_2 have surfaced in the literature by utilizing either the separate reactivity of Lewis acid (LA)/Lewis

Received: February 9, 2016
Published: April 4, 2016

DOI: 10.1021/jacs.6b01497
J. Am. Chem. Soc. 2016, 138, 5321−5333

base (LB) or the combination of them. For instance, Ying et al. reported NHC-catalyzed CO_2 reduction with H_2SiPh_2,[23] while Piers utilized $B(C_6F_5)_3$ (in excess) and TMP for deoxygenative hydrosilylation of CO_2.[24] Müller et al. demonstrated that silyl cations are effective in promoting conversion of CO_2 into benzoic acid, formic acid, and methanol, albeit not in a catalytic fashion.[25] More recently, Wehmschulte et al. reported the LA-catalyzed hydrosilylation of CO_2 by cationic aluminum species AlR_2^+ (R = Et or OAr).[26] However, the detailed mechanism of such LA-catalyzed CO_2 reduction remains unclear, and thus further enhancing catalytic performance through modification of catalyst structure seems challenging. In this context, it is of great interest and importance to survey suitable main-group LA candidates for effective CO_2 reduction. Inspired by the dual activation of CO_2 and silane R_3SiH {[SiH]} by the above overviewed TM or TM/$B(C_6F_5)_3$ systems, we envisioned that a combination of the more oxophilic and higher Lewis acidic $Al(C_6F_5)_3$ {[Al]},[27] which could be sufficiently potent to render CO_2 fixation into silyl formate, with the less oxophilic $B(C_6F_5)_3$ {[B]}, which favors FLP-type [SiH] activation for subsequent steps of reduction,[28] could serve as a main-group tandem FLP system that effectively converts CO_2 to CH_4. The tunability of [Al]/[B] catalysts should allow us to develop more efficient, economical, and recyclable tandem LA catalysts based on inter- or intramolecular and heterogeneous platforms. Accordingly, this contribution reports the first such main-group tandem LA catalytic system for highly effective and selective CO_2 reduction into CH_4 through hydrosilylation using a pair of [Al] and [B] LAs (Chart 1) which, when each used only, is ineffective (in case of [B]) or only marginally effective (in case of [Al]) for catalyzing this transformation. In this context, we present herein a full account of our combined experimental and theoretical/computational investigations into this novel main-group [Al]/[B] tandem catalyst system.

Chart 1. Proposed Fundamental Steps Involved in the Mixed Main-Group [Al]/[B] LA System for Tandem Catalytic Hydrosilylation of CO_2 into CH_4

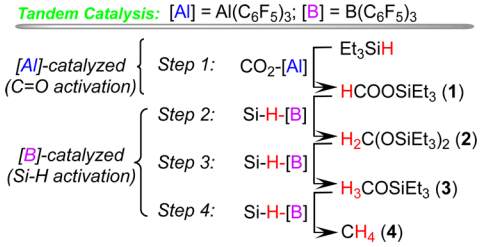

RESULTS AND DISCUSSION

Fixation of CO_2 with {Et_3SiH + [Al]} and Selective Reduction of CO_2 to CH_4 by {Et_3SiH + [Al]/[B]}. As [B] was shown to be ineffective in catalyzing reduction of CO_2 via hydrosilylation,[29] we turned our attention to [Al], a stronger LA based on several lines of experimental and theoretical evidence.[27,30] Most recently, we have revealed that the Al center of the even unsolvated $Al(C_6F_5)_3$ is not truly tricoordinated, but it adopts a dimeric structure with double $Al\cdots F(ortho)$ interactions in solid state.[31] Such weak interactions are readily destroyed by addition of more electron-donating substrates than [Al] itself, such as toluene, ferrocene, or even fluorosilane and hydrosilane.[30a,31,32] For instance, the unsolvated [Al] forms a stable and isolable adduct with Et_3SiH in hexanes, while the interaction between [B] and Et_3SiH could only be detected by indirect spectroscopic evidence.[28h] These observations suggest that the activation of the Si–H bond by [Al] is stronger than by [B]. However, the hydrosilylation of ketones by Et_3SiH proceeds more efficiently with [B] than with [Al], due to the high Lewis acidity and oxophilicity of [Al] that favor its complexation with the ketone substrates, greatly suppressing the Si–H bond activation. On the other hand, the feasible dissociation between the carbonyl substrates and [B] (even at a small ratio) enables the activation of the Si–H bond by the free [B] and the subsequent hydrosilylation.[28j] Notably, Stephan et al. showed that [Al] reacts with CO_2 at 90 °C to form a dimeric Al compound $[(C_6F_5)C(O)OAl(C_6F_5)_2]_2$ by insertion of CO_2 into the Al–C_6F_5 bond,[33] while Müller reported that a [Si–H···Al] system with a coordinatively saturated, less Lewis acidic aluminum center is inactive for CO_2 fixation.[34]

Excitingly, the stoichiometric reaction between [$Et_3SiH\cdot Al(C_6F_5)_3$] and CO_2 at room temperature (RT) (entry 3, Table 1) revealed the rapid disappearance of the silane Si–H signal at 3.75 ppm and concomitant appearance of new signals at 8.17 ppm in ^1H NMR, at 172.8 ppm in ^{13}C NMR, and at 46.0 ppm (downfield shifted from 0.0 ppm from the silane) in ^{29}Si NMR (Figure 1). These spectroscopic features are consistent with the generation of a complexed silyl formate species, which was identified as the complex $HCOOSiEt_3$-[Al] (**1**-[**Al**]), the structure of which was confirmed by single-crystal X-ray diffraction (SC-XRD) analysis (Chart 2). No further reduction to lower oxidation state species was detected. With 10 mol % of [Al], the generation of **1**-[**Al**] (10% based on Et_3SiH) was observed, but no further silane conversion was achieved. Other silanes such as $^iPr_3SiH$ and $PhMe_2SiH$ also led to the formation of the corresponding silyl formate-[Al] complexes (see the Supporting Information). These observations suggest that the activation of CO_2 by [Al] likely occurs through the typical LA-carbonyl activation and the LA is not released from the

Table 1. Selected Results of CO_2 Reduction via Hydrosilylation by [Al] and [Al]/[B]

entry	silane	cat.	conditions	[SiH] conv. (%)[a]	CH_4 yield (%)[b]
1	Et_3SiH	–	12 h, 80 °C	0	0
2	Et_3SiH	5% [B]	12 h, 80 °C	2	0
3	Et_3SiH	100% [Al]	1 h, RT	98	0
4a	Et_3SiH	10% [Al]	10 h, 80 °C	39	14
4b	Et_3SiH	10% [Al]	24 h, 80 °C	54	16
5	Et_3SiH	5.0% [Al] + 5.0% [B]	1 h, RT	15	7
6	Et_3SiH	5.0% [Al] + 5.0% [B]	5 h, 80 °C	**100**	**82**

[a]Based on silane consumption. [b]See the SI for yield calculation details.

DOI: 10.1021/jacs.6b01497
J. Am. Chem. Soc. 2016, 138, 5321–5333

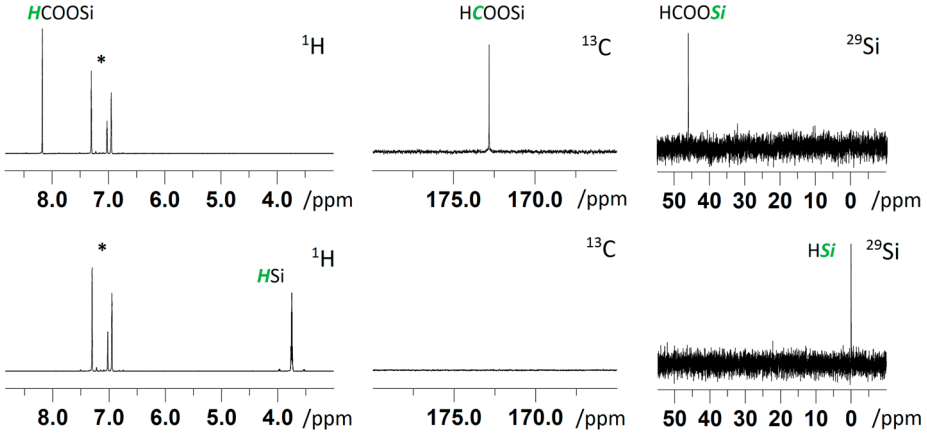

Figure 1. Comparisons of ^{1}H, ^{13}C, and ^{29}Si NMR spectra before (bottom) and after (top) CO_2 fixation by [Et_3SiH + $Al(C_6F_5)_3$] in C_6D_5Br at 25 °C.

Chart 2. CO_2 Insertion into Si−H Bond with the [Et_3SiH + $Al(C_6F_5)_3$] System To Form the [Al]-Coordinated Silyl Formate and the Corresponding Solid-State Structure Determined by SC-XRD

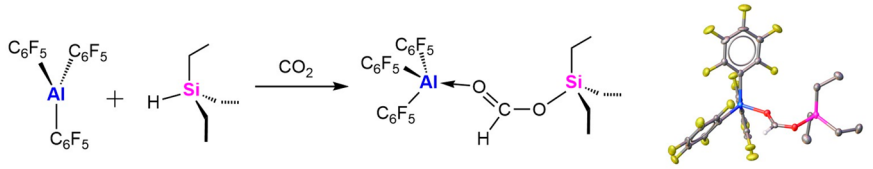

resulting product under these conditions, thus requiring a stoichiometric amount of LA. To render this reaction catalytic and possibly promote further hydrosilylation of the formed intermediates, we heated the above mixture to 80 °C for 24 h, achieving a moderate conversion of 54% (calculated from the silane consumption) with a 16% CH_4 yield (entry 4b, Table 1). These results imply that the catalytic performance of [Al] decreases as the basicity of the subsequent reaction intermediates [$HCOOSiEt_3$, $H_2C(OSiEt_3)_2$, and $H_3COSiEt_3$, vide infra] increases. Intriguingly, when we employed a mixed LA system containing 5 mol % [Al] + 5 mol % [B], quantitative conversion of the silane with 82% CH_4 yield was achieved at 80 °C in 5 h (entry 6, Table 1; Figure 2).

Isolation of Reaction Intermediates. To elucidate the possible mechanism for this unique [Al]/[B] tandem catalyst system, we synthesized each of the intermediates or byproducts involved in the above reduction scheme, including $HCOOSiEt_3$, $H_2C(OSiEt_3)_2$, $H_3COSiEt_3$, and $Et_3SiOSiEt_3$ (Scheme 1).

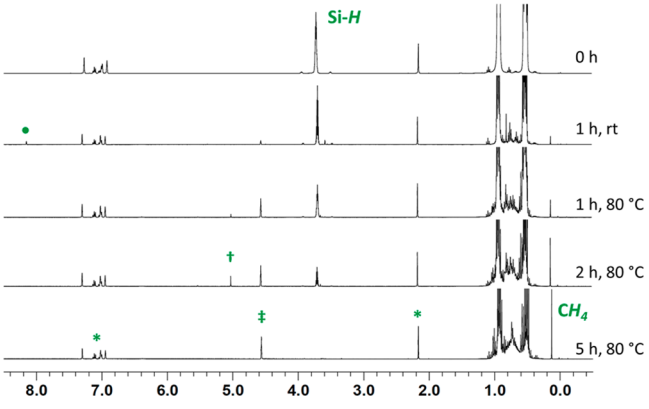

Figure 2. ^{1}H NMR (25 °C, C_6D_5Br) spectra of hydrosilylation of CO_2 catalyzed by the mixed Al/B system (entries 5 and 6, Table 1) at different time intervals (●: $HCOOSiEt_3$-[Al], ‡: $H_2C(OSiEt_3)_2$-[Al], †: free $H_2C(OSiEt_3)_2$ and *: toluene from [Al] and NMR solvent residue).

Scheme 1. Preparation of the Reaction Intermediates Involved in the Overall CO_2 Reduction Cycle

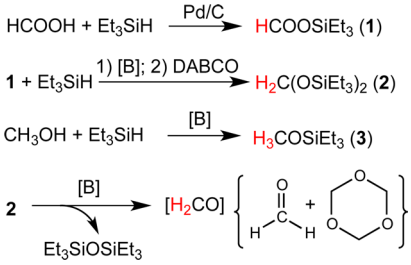

Compounds $HCOOSiEt_3$ and $H_3COSiEt_3$ were readily prepared from the dehydrogenative coupling of the corresponding precursors by Pd/C or [B].[26b] On the other hand, successful examples or selective formation and isolation of $H_2C(OSiEt_3)_2$ remain scarce.[5a,15,16] Piers et al. noted that the sequestration of the [B] catalyst to prevent further hydrosilylation is necessary.[16a] Interestingly, in our attempts to reduce $HCOOSiEt_3$ with 1 equiv of Et_3SiH, we observed selective formation of $H_2C(OSiEt_3)_2$ in 5 min, after which the product gradually underwent further rearrangement to form 1,3,5-trioxane (a formaldehyde equivalent) and hexaethyldisiloxane $Et_3SiOSiEt_3$. This process is believed to proceed through coordination of the catalytic amount of [B] to the substrate, as sequestration of [B] with DABCO (1,4-diazabicyclo[2.2.2]-octane) prevented the aforementioned rearrangement reaction and enabled the isolation of $H_2C(OSiEt_3)_2$. In a separate NMR scale experiment, $H_2C(OSiEt_3)_2$ was left for 1 day in C_6D_5Br and remained intact, but addition of 5 mol % of [B] converted $H_2C(OSiEt_3)_2$ into 1,3,5-trioxane and $Et_3SiOSiEt_3$ in 1 h

DOI: 10.1021/jacs.6b01497
J. Am. Chem. Soc. 2016, 138, 5321−5333

Scheme 2. Binding Interaction of Each Intermediate with [Al] and [B] Catalysts

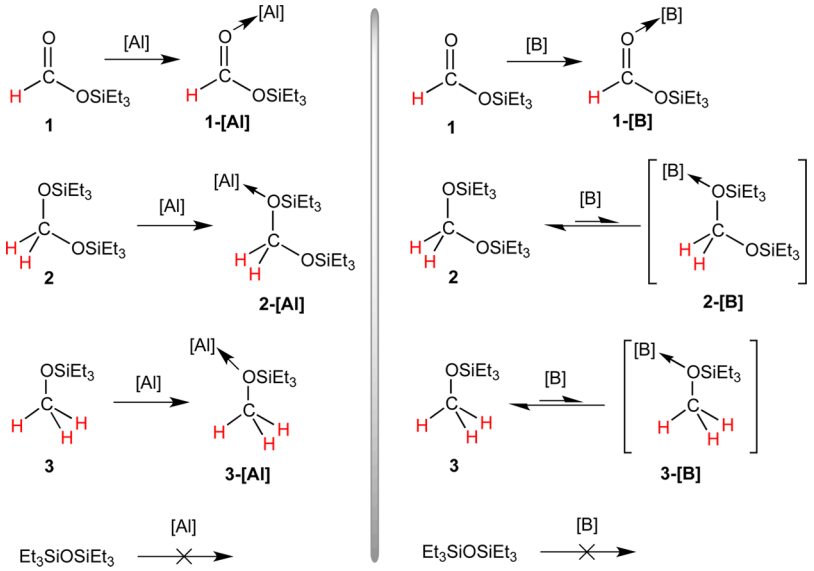

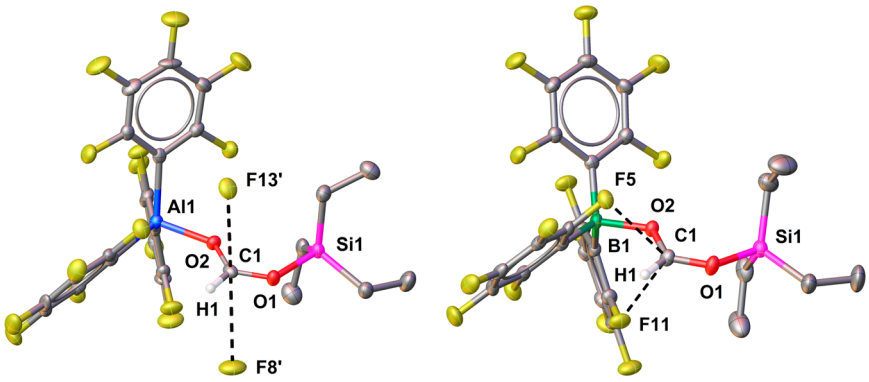

Figure 3. X-ray crystal structures of **1**-[**Al**] and **1**-[**B**] with thermal ellipsoids drawn at the 50% probability. Hydrogen atoms except H1 were omitted for clarity. Selected bond lengths (Å) and angles (deg) for **1**-[**Al**]: C1−O1 1.277(2), C1−O2 1.242(2), Al1−O2 1.8532(16), Si1−O1 1.7717(15), C1···F8′ 2.935(3), and C1···F13′ 2.908(3); for **1**-[**B**]: C1−O1 1.276(2), C1−O2 1.245(2), B1−O2 1.621(2), Si1−O1 1.7499(14), C1···F5 2.838(3), and C1···F11 2.748(2).

(Figures S21 and S22). Indeed, the formation of the formaldehyde intermediate even without a catalyst is energetically feasible for bis(phenylsilyl)acetal $H_2C(OSiH_2Ph)_2$, via intramolecular elimination of $PhH_2SiOSiH_2Ph$, as predicted by calculations reported by Wang et al.[35] Our proposed mechanism through coordination of $H_2C(OSiEt_3)_2$ to [B] will be discussed in the following sections. The final disiloxane product of CO_2 reduction, $Et_3SiOSiEt_3$, can also be isolated as the byproduct by vacuum distillation.

Binding Interaction between the Intermediates and [Al] or [B]. With all three intermediates in hand, we studied their interaction with [Al] and [B] (Scheme 2). As expected, the less sterically hindered $HCOOSiEt_3$ forms a stable adduct with both [Al] and [B]. Crystalline **1**-[**Al**] and **1**-[**B**] adducts can be isolated in pure form by crystallization of equimolar **1** and [Al] or [B] in hexanes at −30 °C. Further supporting evidence came from multinuclear spectroscopic data (Figures S1−9) chiefly: (1) the aldehyde proton appears at 8.17 and 7.95 ppm in ^{1}H NMR for **1**-[**Al**] and **1**-[**B**], respectively; (2) the ^{19}F NMR spectra also exhibit typical patterns for tetracoordinate aluminum and boron species; (3) both the formate and the LA signals are present in the ^{13}C NMR and assigned; and (4) the ^{29}Si NMR signals are significantly downfield shifted for **1**-[**Al**] (δ 46.0 ppm) and **1**-[**B**] (δ 46.4 ppm) when compared to the free **1** (δ 26.5 ppm). Worth noting here is that the spectroscopic data of **1**-[**Al**] is consistent with those generated by the stoichiometric reaction between CO_2 and $[Et_3SiH{\cdot}Al(C_6F_5)_3]$.

The direct structural evidence for the 1:1 complexation in **1**-[**Al**] and **1**-[**B**] was derived from the SC-XRD analysis (Figure 3). In the structure of **1**-[**Al**], the Al−O2 bond is rather strong, as indicated from the short bond length of 1.8532(16) Å. Notably, the C1−O2 and C1−O1 distances are 1.242(2) and 1.277(2) Å. This specific alternation suggests that C1−O2 features a more double-bond character, while C1−O1 features a more single-bond character. In another word, if **1**-[**Al**] is viewed as a model in which [Al] and $[Si]^+$ are competing for the middle formate anion, then $[Si]^+$ exhibits stronger interaction with the anion. Nonetheless, both C1−O2 and C1−O1 distances are shorter than the typical C−O single bond (cf. 1.43 Å) and longer than the C═O double bond (cf. 1.23 Å), indicative of a certain degree of conjugated resonance structure along the −O1−C1−O2− moiety. The middle C1 carries a partial positive charge, accounting for the further secondary interactions with two *para*-F atoms [C1···F contact: 2.908(3) and 2.935(3) Å] from two neighboring molecules.

DOI: 10.1021/jacs.6b01497
J. Am. Chem. Soc. 2016, 138, 5321−5333

Scheme 3. Catalytic Hydrosilylation Reaction of Each Fundamental Step

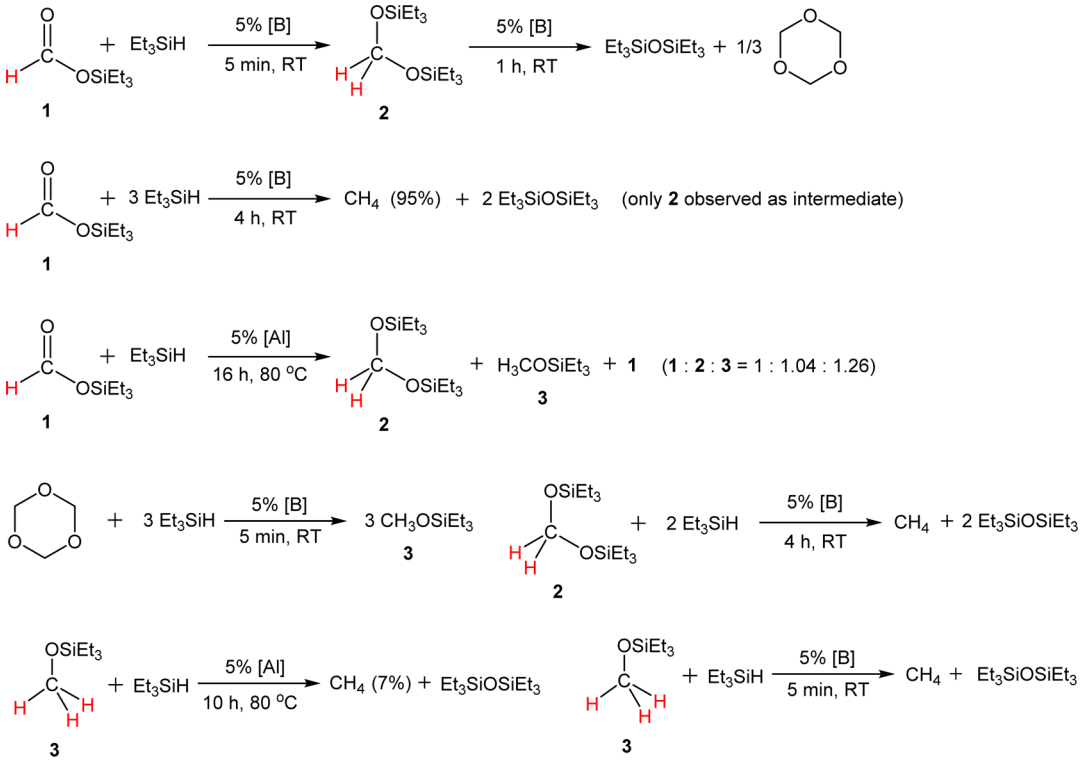

The structural parameters for **1**-[**B**] are overall similar to those of **1**-[**Al**]: C1−O1 1.276(2), C1−O2 1.245(2), B1−O2 1.621(2), except that secondary C···F contacts [2.748(2) and 2.838(3) Å] were derived from an intramolecular fashion with the adjacent $-C_6F_5$ ring instead, presumably due to the smaller radius of boron and shorter bond lengths around it. Further evidence for activation of the carbonyl moieties by LAs was deduced from FT-IR analysis of the solid samples of **1**-[**Al**] and **1**-[**B**] (Figure S32). When compared with the uncoordinated **1** (cf. 1708 cm^{-1}), both **1**-[**Al**] (1604 cm^{-1}) and **1**-[**B**] (1597 cm^{-1}) exhibit significant shifts of the C═O stretching mode to lower frequencies by 104 and 111 cm^{-1}, respectively.

In contrast, the interaction of [Al] and [B] with the bulkier and less basic $H_2C(OSiEt_3)_2$ and $H_3COSiEt_3$ is different (see Scheme 2 and SI). In the case of the more sterically hindered and less acidic [B] (relative to [Al]), there was no spectral change from the ^1H NMR signals for its 1:1 mixture with $H_2C(OSiEt_3)_2$ or $H_3COSiEt_3$. However, based on the fact that $H_2C(OSiEt_3)_2$ readily undergoes the rearrangement reaction in the presence of [B] in a prolonged period, it is likely that [B] can bind to $H_2C(OSiEt_3)_2$, albeit in a very weak fashion that favors the dissociated form. Given that the bulkiness of $H_3COSiEt_3$ is less than that of $H_2C(OSiEt_3)_2$, it is plausible that [B] can also bind to $H_3COSiEt_3$ reversibly, even though the ^1H data again indicated that this equilibrium strongly favors the dissociated form. To the contrary, the NMR scale reaction between [Al] and $H_2C(OSiEt_3)_2$ or $H_3COSiEt_3$ results in spectral shifts in the ^1H signals, corresponding to complexation between [Al] and $H_2C(OSiEt_3)_2$ or $H_3COSiEt_3$. In particular, [Al] forms isolable crystalline complex with $H_3COSiEt_3$. We tried to perform SC-XRD analysis of the complex but failed to obtain satisfactory results after several attempts due to poor crystal quality. Nonetheless, the overall molecular skeleton and atom connectivity of this adduct could be recognized from the crude data (Figure S34). Collectively, these observations further support that in the subsequent reduction of lower-oxidation-state species $HCOOSiEt_3$, $H_2C(OSiEt_3)_2$, and $H_3COSiEt_3$, [B] should serve as a better catalyst than [Al] due to the weaker substrate−catalyst interaction, which facilitates the FLP-type Si−H activation. In addition, the byproduct $Et_3SiOSiEt_3$ does not form a detectable adduct with either [B] or [Al], which enables [Al] and/or [B] to re-enter the catalytic cycle after the last step (CH_4 generation).

Kinetic and Mechanistic Studies of Hydrosilylation of CO_2. To further address our hypothesis on the catalytic roles of each LA in the current mixed tandem [Al]/[B] system, we carried out a kinetic study on each step of the hydrosilylation (Scheme 3), coupled with a computational investigation (vide infra). As described previously, in step 1, the fixation of CO_2 is mediated by [Al] to form **1**-[**Al**]. The following hydrosilylation steps 2−4 proceed more efficiently with [B] than with [Al]. Among them, the reactions of $HCOOSiEt_3$ or $H_3COSiEt_3$ with 1.0 equiv of Et_3SiH in the presence of 5 mol % [B] were completed within 5 min at RT, while the slowest step, the hydrosilylation of $H_2C(OSiEt_3)_2$ under similar conditions generated a mixture of unreacted $H_2C(OSiEt_3)_2$, CH_4, and a trace amount of $H_3COSiEt_3$. Nonetheless, treatment of $HCOOSiEt_3$ with 3.0 equiv of Et_3SiH and 5 mol % [B] resulted in almost quantitative conversion to CH_4 in 4 h, during which $H_2C(OSiEt_3)_2$ accumulates as the detectable intermediate. In addition, the reduction of 1,3,5-trioxane with 1.0 equiv of Et_3SiH and 5 mol % [B] led to exclusive formation of $H_3COSiEt_3$, indicating that the hydrosilylation of trioxane is even faster than that of $H_3COSiEt_3$. In comparison, the hydrosilylation of the related substrates with [Al] at RT is not effective at all and only provided a trace amount of the reduction products, but at 80 °C after longer times some hydrosilylation products were observed (Scheme 3)

DOI: 10.1021/jacs.6b01497
J. Am. Chem. Soc. 2016, 138, 5321−5333

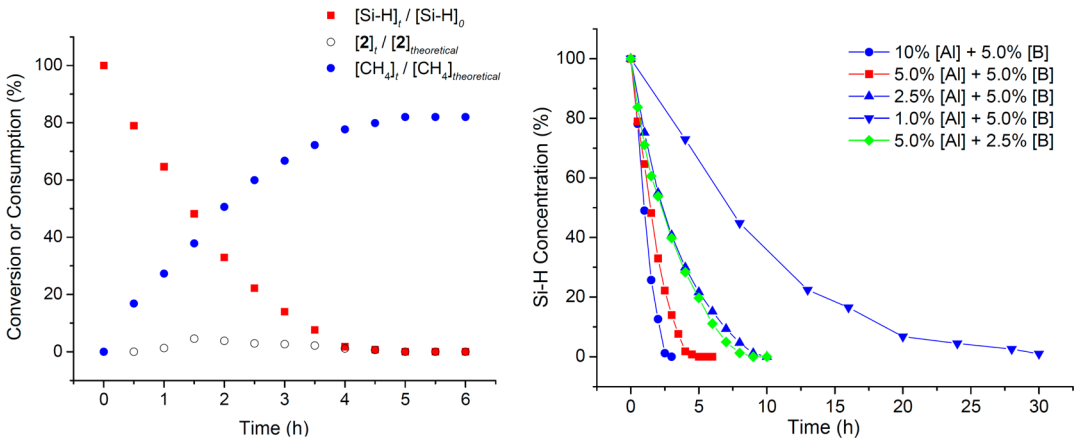

Figure 4. Kinetic plots under current standard conditions (left, 80 °C, 5 mol % [Al], and 5 mol % [B]) and varied loading of [Al] and [B] (right).

Table 2. Selected Results of CO_2 Hydrosilylation at 80 °C under Different Tandem Catalyst Loadings

catalyst composition	reaction time (h)[a]	max TOF (h^{-1})[b]	r_{SiH} (M h^{-1})[c]	conv. (%)[d]	CH_4 yield (%)[e]
10% [Al] + 5.0% [B]	3	5.0	0.20	100	77
5.0% [Al] + 5.0% [B]	5	6.6	0.13	100	82
2.5% [Al] + 5.0% [B]	10	7.9	0.079	100	91
1.0% [Al] + 5.0% [B]	30	6.03	0.024	**99**	**94**
5.0% [Al] + 2.5% [B]	9	7.85	0.0785	100	80

[a]Based on [SiH] consumption from ^{1}H NMR measurement. [b]Based on the steepest slope from the linear fit of conversion against time at the early stage of hydrosilylation, see Figures S27–S31. [c]Rate of [SiH] consumption, calculated based on max TOF. [d]Based on [SiH] consumption. [e]See the SI for yield calculation details.

To gain further insights of such tandem hydrosilylation of CO_2, we carried out a kinetic study of the overall reduction process. Under our standard conditions (entry 6, Table 1), the reaction was complete in 5 h. Et_3SiH consumption and CH_4 yield at the early stage of the reaction showed a linear relationship with time (Figure 4). The concentration of detectable intermediate $H_2C(OSiEt_3)_2$ (**2**) reached a plateau at 1.5 h and then decreased gradually. The maximum turnover frequency (TOF) of the consumption of [SiH] using the first 5 data points from the initial 2 h was calculated to be 6.6 h^{-1}, and the rate for the [SiH] conversion was r_{SiH} = 0.13 M h^{-1}. Variation of the [Al] catalyst concentration (from 1.0 mol % to 10 mol %, Table 2) greatly impacted the [SiH] consumption rate. Overall, the reduction rate of CO_2, as monitored by the consumption of [SiH] signal, was proportional to the [Al] loading. The only observed species at δ 4.57 ppm after complete [SiH] conversion was the **2**-[**Al**] adduct, which is consistent with the stoichiometric reaction between **2** and [Al]. As expected, lowering the [Al] loading reduced the amount of the final **2**-[**Al**] residue and hence improved the yield of CH_4. In addition, decreasing the [B] concentration also resulted in a decrease of CO_2 reduction rate. Remarkably, when only 1.0 mol % of [Al] was employed, the highest CH_4 yield of 94% was achieved (Table 2).

Collectively, the above results showed that CO_2 fixation is promoted by [Al], while the subsequent hydrosilylation reactions are catalyzed by [B]. To further clarify the preferred pathway of each step, namely conventional carbonyl activation versus FLP-type silane activation, and to explain the observed activity for the CO_2 reduction into CH_4 by [Al] alone but requiring 80 °C for 24 h (entries 4a-b, Table 1), albeit being much less effective than the mixed [Al]/[B] tandem catalyst system, we performed the following additional experiments. We first mixed equimolar **1**-[**B**] and Et_3SiH-[Al], which resulted in the instantaneous replacement of Et_3SiH by $HCOOSiEt_3$ to form **1**-[**Al**]. However, the subsequent hydrosilylation was hindered, as only a trace amount of **2**-[**Al**] was detected up to 1 h, in contrast to the rapid reduction of **1**-[**B**] by Et_3SiH in the absence of [Al]. This observation is in line with the Si–H activation mechanism, in which the free carbonyl has to be formed to initiate the attack at the Si center of a transient Si–H···[B] intermediate. If the carbonyl is coordinated to an additional LA, [Al], such nucleophilic attack becomes less plausible. With this premise, we gratifyingly found that heating the mixture to 80 °C led to the formation of **2**-[**Al**], due to thermally induced dissociation of $HCOOSiEt_3$ from [Al], enabling its reduction to $H_2C(OSiEt_3)_2$ that recombines with [Al] to form **2**-[**Al**]. Addition of an excess amount of Et_3SiH into such a mixture further converted $H_2C(OSiEt_3)_2$ to CH_4 at 80 °C. In a similar fashion, addition of [Al] to a mixture of $H_3COSiEt_3$, [B] and Et_3SiH reduced the hydrosilylation rate of $H_3COSiEt_3$ to CH_4. These experiments further confirm that the reduction steps 2–4 occur through the FLP Si–H activation mechanism, and a higher temperature is necessary to facilitate the release of substrates (**1**, **2**, and **3**) from [Al], which also renders [Al] catalytic by reentering the catalytic cycle for the step 1 reduction.

In order to investigate the catalyst recyclability, the catalytic system consisting of 10 mol % [Al] and 5.0 mol % [B] was tested for 3 cycles. In the first cycle, the hydrosilylation was complete in 3 h (Figure 5). After careful removal of excess CO_2 and CH_4 under vacuum, the system was recharged with the same amount of Et_3SiH and CO_2 as in the first cycle. The hydrosilylation of the second and third cycles was complete in 6 and 14 h, respectively. This recycling experiments indicated that the [Al]/[B] catalysts survived during catalytic cycle and are recyclable. Although we detected the decrease in catalyst efficiency from cycle to cycle (presumably due to partial

DOI: 10.1021/jacs.6b01497
J. Am. Chem. Soc. 2016, 138, 5321–5333

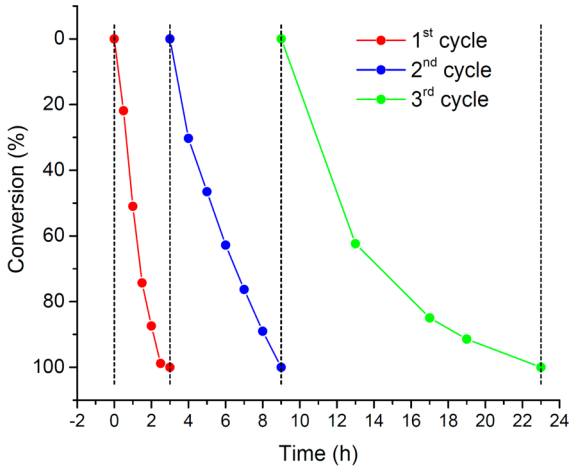

Figure 5. Recyclability of CO_2 reduction with 10 mol % [Al] and 5.0 mol % [B]. Reaction time for complete SiH consumption in each cycle: 3, 6, and 14 h.

hydrolysis of the catalyst during the reloading of CO_2), quantitative conversion can still be achieved on the third load of Et_3SiH and CO_2.

Computational Studies of Fundamental Steps 1−4.[36] In this section we discuss each reduction step separately starting from the hydrosilylation of CO_2 to formate and ending with the hydrosilylation of methyl silyl ether to methane. In Schemes 4, 5, and 6 numbers in green refer to [Al], while numbers in blue refer to [B]. Further, to strengthen connections with experiments, we labeled DFT structures using letters, such as **A**, **B**, **C**, etc., while for structures involving intermediates **1**−**3** we kept the same labeling scheme as that used in the description of the experimental results.

Step 1: Hydrosilylation of CO_2 to Silylformate 1-[X] (X = Al, B). The two possible reaction pathways we investigated to generate **1** from CO_2 are reported in Scheme 4.

Along pathway 1 the individual LA directly activates the CO_2 molecule toward the H-transfer from Et_3Si−H. Pathway 2, instead, starts with a FLP-type Si−H activation with coordination of Et_3SiH to the LA, followed by the H-transfer to the CO_2 molecule through an insertion mechanism or a SN_2 transition state and by rearrangement of the initially formed $[OCOSiEt_3]^+/[H\text{-}LA]^-$ ion pair. Focusing on pathway 1, in the case of [B] we were not able to locate a CO_2-$B(C_6F_5)_3$ adduct, **B**. Nevertheless, we found two possible four-membered transition states, **B**/**C** and **B**/**1**-[**X**] in Scheme 4, where the silicon attacks one oxygen of CO_2 favoring the simultaneous H-transfer from Et_3Si−H to the CO_2 carbon atom. Transition state **B**/**C** collapses into intermediate **C** before reaching **1**-[**X**], favored by 9.4 kcal/mol, while transition state **B**/**1**-[**X**] collapses directly into product **1**-[**X**]. The energy cost to reach transition states **B**/**1**-[**X**] and **B**/**C**, around 35−39 kcal/mol, and the fact that these transition states should be formed by the encounter of three molecules due to the instability of the preformed **B** intermediate explain the experimentally observed inability of [B] to activate CO_2. Conversely, the CO_2-alane adduct **B** was located 6.5 kcal/mol below separated $Al(C_6F_5)_3$ and CO_2. This interaction weakens the C═O bond of the CO_2 moiety, as shown by the slightly elongated C═O bond distance (1.19 Å in **B** vs 1.17 Å in the free CO_2). [Al] coordination results in an increased positive charge on the C atom of the CO_2 moiety (1.07e in **B** vs 0.99e in the free CO_2), promoting the H-transfer from Et_3SiH to the electrophilic C center. This H-transfer occurs via the four-membered transition state **B**/**C**, with the [Al] coordinated O atom attacking the Si atom and an energy barrier of 22.0 kcal/mol. Transition state **B**/**C** collapses into intermediate **C**, which can further precipitate in the final product **1**-[**X**] (ΔG = −28.8 kcal/mol) through the almost barrier-less transfer of the [Al] to the carbonyl oxygen, via transition state **C**/**1**-[**X**]. The alternative transition state with the uncoordinated O atom of **B** attacking the Si atom, **B**/**1**-[**X**], and leading to **1**-[**X**] directly, was located 3.5 kcal/mol above **B**/**C**. The stability of the CO_2-[Al] adduct **B** and the low-energy barrier of 22.0 kcal/mol explain the experimentally observed capability of [Al] to activate CO_2.

As for the competitive mechanism via Si−H activation, pathway 2 in Scheme 4, it involved the formation of a silane-LA adduct. Formation of such adduct was found to be favored by 7.2 kcal/mol with [Al], whereas in the case of [B] it is

Scheme 4. Hydrosilylation of CO_2 to the Silylformate Complex 1-[X][a]

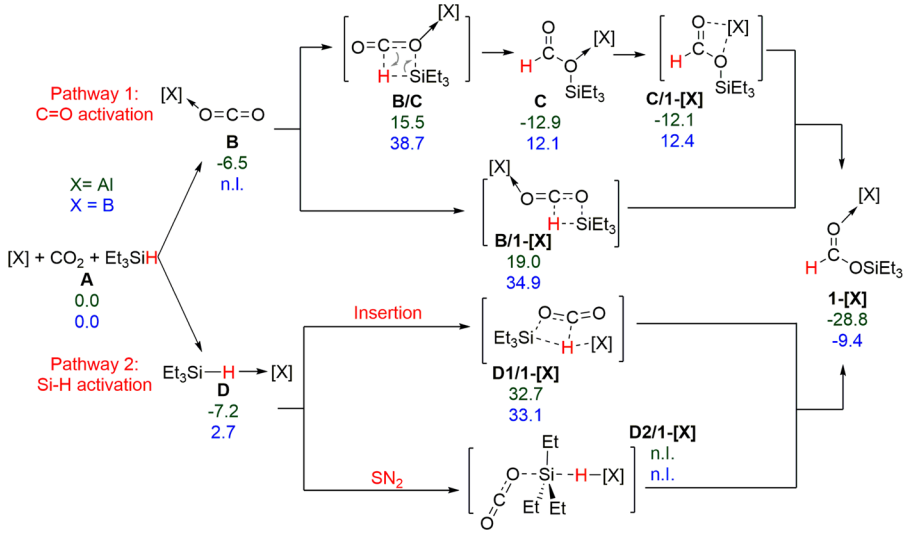

[a]Free energies (kcal/mol) in *n*-Hexane are reported for X = Al (numbers in green) and B (numbers in blue) (n.l. = not located).

DOI: 10.1021/jacs.6b01497
J. Am. Chem. Soc. 2016, 138, 5321−5333

Scheme 5. Hydrosilylation of Silylformate 1-[X] to $H_2C(OSiEt_3)_2$/Formaldehyde[a]

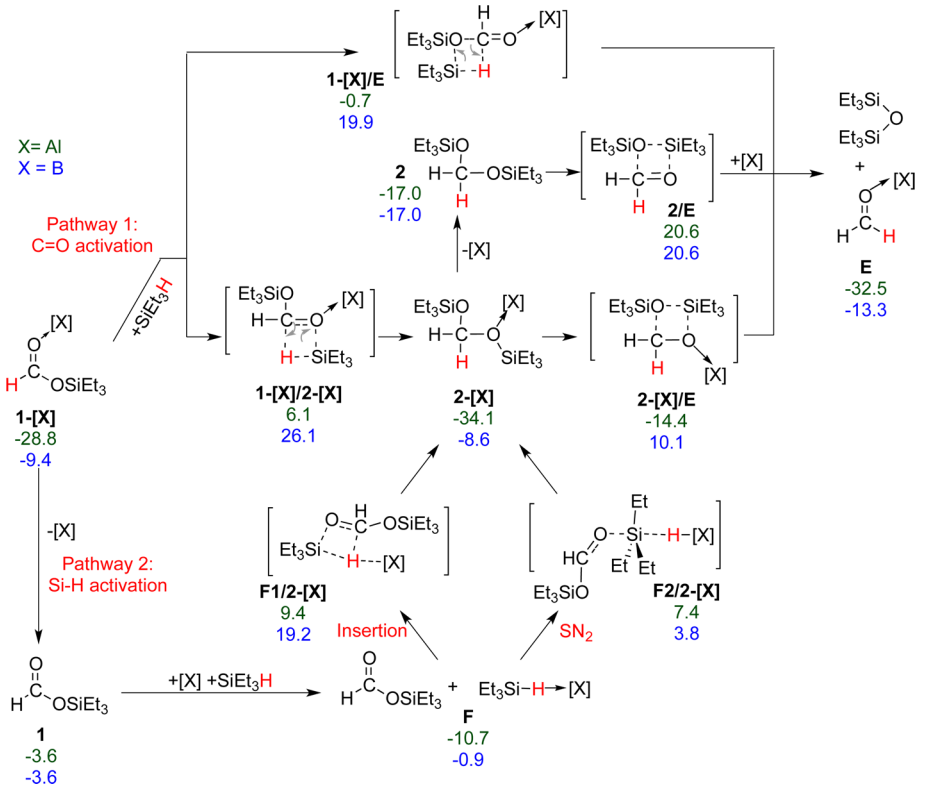

[a]Free energies (kcal/mol) in *n*-hexane are reported for X = Al (numbers in green) and B (numbers in blue).

disfavored by 2.7 kcal/mol. The transition state for the following insertion of CO_2 into the Si−H bond, **D1**/**1**-[X] in Scheme 4, lies at 32.7 kcal/mol for [Al] and 33.1 kcal/mol for [B]. Finally, we also tried to promote Si−H activation via the SN_2-type transition state **D2**/**1**-[X], corresponding to the concerted attack of the CO_2 oxygen to the silicon atom and transfer of the H atom to the [X] moiety. However, we were not able to locate this kind of transition state for both [Al] and [B]. Overall, calculations confirmed the experimental inefficiency of [B] in the first step of CO_2 hydrosilylation, since [B] is not able to effectively activate CO_2 through either direct coordination to CO_2 or FLP-type silane activation. As far as [Al] is concerned, calculations suggest that the reduction of CO_2 to silylformate occurs via CO_2 activation, whereas the pathway involving the FLP-type Si−H activation was ruled out.

Steps 2 and 3a: Hydrosilylation of Silylformate 1-[X] to $H_2C(OSiEt_3)_2$ (Step 2) and Formaldehyde (Step 3a). Starting from the LA-silylformate adduct **1**-[X], we studied the mechanisms most likely operative in the second hydrosilylation step, namely from the silylformate adduct **1**-[X] to fomaldehyde. The pathways considered with the corresponding energetics are reported in Scheme 5. We considered the H-transfer step from a second Et_3SiH molecule to the starting **1**-[X] via the same pathways considered above for hydrosilylation of CO_2. Specifically, we considered two transition states along the C═O activation pathway, i.e., **1**-[X]/**E** and **1**-[X]/**2**-[X], where the Et_3SiH molecule attacks the oxygen of the LA−O bond or the oxygen of the Si−O bond of **1**-[X]. Transition state **1**-[X]/**E**, leading directly to $Et_3SiOSiEt_3$ and the LA-aldehyde adduct, **E** in Scheme 5, is favored by roughly 6−7 kcal/mol relative to transition state **1**-[X]/**2**-[X], leading to adduct **2**-[X], with the experimentally characterized $CH_2(OSiEt_3)_2$ intermediate **2** bound to the LA. In this conversion, the two LAs behave similarly, with an overall energy barrier through the favored transition state **1**-[X]/**E** of roughly 29 kcal/mol. This relatively high-energy barrier can be ascribed both to the high steric pressure in this second hydrosilylation transition state (two molecules of silane plus one LA) and to the reduced electrophilicity of the formate carbon center with respect to that of CO_2, as revealed by the charges of these two C centers, i.e., 1.07e in CO_2 vs 0.74e in **1**-[X]. Finally, formation of **E** from **1**-[X] + Et_3SiH is exergonic by almost 4.0 kcal/mol for both LAs, which drives aldehyde formation. As for conversion of the experimentally characterized intermediate **2**-[X] to the formaldehyde adduct **E**, it can proceed either in a single step through transition state **2**-[X]/**E** or through a two-step pathway via dissociation of [X] from **2**-[X], followed by the direct reductive elimination of $Et_3SiOSiEt_3$ from **2** to release the aldehyde via transition state **2**/**E**, following a similar mechanism reported in literature.[35] According to our calculations, the one-step mechanism via transition state **2**-[X]/**E**, with an overall energy barrier around 20 kcal/mol, is clearly favored over the direct reductive elimination from **2**. Nevertheless, dissociation of the LA from **2**-[X] releasing intermediate **2** is energetically favored with [B], actually representing the thermodynamic product of the reaction.

As for the Si−H activation pathway, it starts with the conversion of **1**-[X] into **2**-[X], with the steps from **2**-[X] to **E** already being discussed above. Thus, we focus here on the pathway from **1**-[X] to **2**-[X]. We calculated first the energetics involved in the release of the LA from the silylformate adduct **1**-[X]. As expected, dissociation of [Al], with a ΔG of 25.2 kcal/mol, is more expensive than dissociation of [B], with a ΔG

DOI: 10.1021/jacs.6b01497
J. Am. Chem. Soc. 2016, 138, 5321−5333

Scheme 6. Hydrosilylation of Formaldehyde to Silyl Methanol and Then to Methane[a]

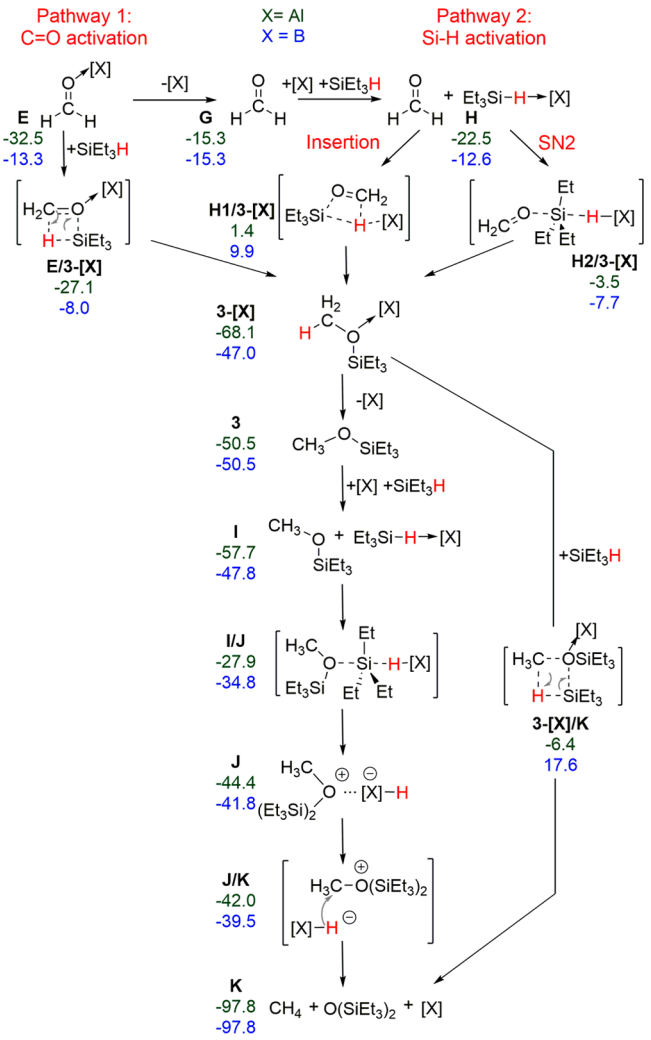

[a]Free energy (kcal/mol) in *n*-hexane are reported for X = Al (numbers in green) and B (numbers in blue).

of only 5.8 kcal/mol. Starting from the LA free species **1** and a preformed Et_3SiH-[X] adduct, we located both the transition states for the direct formate insertion into the Si−H bond, **F1/2-[X]**, and the direct H-transfer between Et_3SiH and the LA via SN_2-type reactivity, **F2/2-[X]**. Based on the energy of the H-transfer transition states, both the Si−H activation pathways we examined can be ruled out in the case of [Al], since transition states **F1/2-[X]** and **F2/2-[X]** are more than 35 kcal/mol above intermediate **1-[X]**. Conversely, the insertion Si−H activation pathway is isoenergetic with the C═O activation pathway in the case of [B] and, more relevantly, the SN_2 type H-transfer mechanism via transition state **F2/2-[X]** shows a barrier of only 13.2 kcal/mol.

Focusing on the thermodynamic scenario, the stability of the intermediates shown in Scheme 5 seems to correlate with the different catalytic behavior in the presence of [Al] or [B]. In fact, for [Al] the thermodynamic product is the $H_2C(OSiEt_3)_2$-[Al] adduct **2-[X]**, which is favored by 1.6, 5.3, and 17.1 kcal/mol relative to **E**, **1-[X]**, and **2**, respectively. As consequence, liberation of [Al] to promote further reactivity is compromised. On the contrary, intermediate **2** is the most stable species in the presence of [B], followed by **E**, with **1-[X]** and **2-[X]** being clearly much less stable. The different thermodynamic stability of **2** and **2-[X]** with [Al] and [B], together with the much lower energy barrier via the Si−H activation pathway, renders the [B] catalyst active in the reduction of silylformate to formaldehyde, in agreement with the experimental results.

Steps 3b and 4: Hydrosilylation of Formaldehyde to Silyl Methanol (Step 3b) and Then to Methane (Step 4). The reaction pathways we considered for the last two steps to form methane from the aldehyde-LA adduct **E** are reported in Scheme 6 with the related energies. Since no favored hydrosilylation pathway was located starting from **2** of Scheme 5, we focused on the aldehyde-LA adduct **E** that turns out to be the crucial species for the course of the reaction. Intermediate **E** can react with the third equivalent of Et_3SiH along the C═O activation pathway via the low-energy H-transfer transition state **E/3-[X]** with both the LAs considered, with an energy barrier around 5 kcal/mol. Alternatively, the key intermediate **3-[X]** can also be reached from **E** along the Si−H activation pathway after dissociation of the LA to reach intermediate **G**. As calculated in the previous reaction sequences, dissociation of [Al] from **E** is clearly endergonic, whereas it is favored with [B]. The liberated formaldehyde can react with a Et_3SiH-LA adduct, intermediate **H**, via the already considered insertion or SN_2-type pathways, through transition states **H1/3-[X]** and **H2/3-[X]**, respectively. The insertion mechanism can be excluded since the **H1/3-[X]** transition state is more than 20 kcal/mol higher in energy than transition state **E/3-[X]** for both [Al] and [B]. As for the SN_2-type pathway, it is competitive for [B], since transition state **H2/3-[X]** is almost isoenergetic with transition state **E/3-[X]** along the C═O activation pathway. Differently, it can be excluded for [Al] since the transition state **H2/3-[Al]** is almost 24 kcal/mol higher in energy than transition state **E/3-[Al]**.

Two different pathways were considered to generate methane from **3-[X]**. The first pathway is the one-step H-transfer from the fourth equivalent of Et_3SiH molecule to the carbon of the activated adduct **3-[X]** (C−O activation pathway) via transition state **3-[X]/K**. This pathway can be excluded, since it requires the overcome of an energy barrier >60 kcal/mol (Scheme 6). The second pathway is a multistep process and starts with release of the LA from **3-[X]**, which is again strongly endergonic for [Al], whereas it is slightly exergonic for [B] (**3-[X]** vs **3** for [Al] and [B] in Scheme 6). After releasing LA from **3-[X]**, silyl methanol **3** proceeds to the last hydrosilylation step, via SN_2-type transition state **I/J** involving **3** and a Et_3SiH-LA adduct. This H-transfer step is rate determining, with a barrier of 16.0 kcal/mol for [B] (calculated from the most stable **3** + Et_3SiH + LA species) and of almost 40 kcal/mol for [Al] (calculated from the most stable **3-[X]** + Et_3SiH species). As a consequence and in agreement with the experimental results, the [Al] catalyst is inactive also in this last hydrosilylation step, which proceeds smoothly with the [B] catalyst. The last H-transfer within the formal $[CH_3O\text{-}(Et_3Si)_2]^+/[H\text{-LA}]^-$ adduct **J** to release methane via transition state **J/K** is almost barrier-less. As expected, formation of methane is thermodynamically favored by roughly 50 kcal/mol with respect to the silyl methanol intermediate **3**. For the sake of simplicity, the insertion pathway is not reported for the conversion of **3** to methane, since it involves a clearly unfeasible barrier, as discussed in the previous sections.

Alane vs Borane: Electronic and Steric Analysis. The results reported in the previous sections showed that the experimentally observed catalytic difference between [Al] and

DOI: 10.1021/jacs.6b01497
J. Am. Chem. Soc. 2016, 138, 5321−5333

Scheme 7. Four Fundamental Steps and Calculated Energy Barriers in the Proposed Complete Catalytic Cycle for the Hydrosilylation of CO_2 into CH_4 in the Presence of Mixed [Al] and [B] LAs

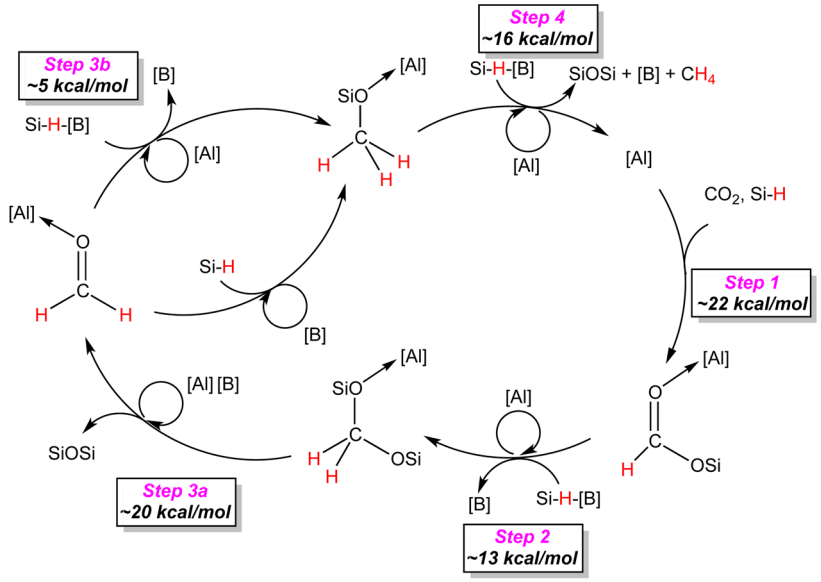

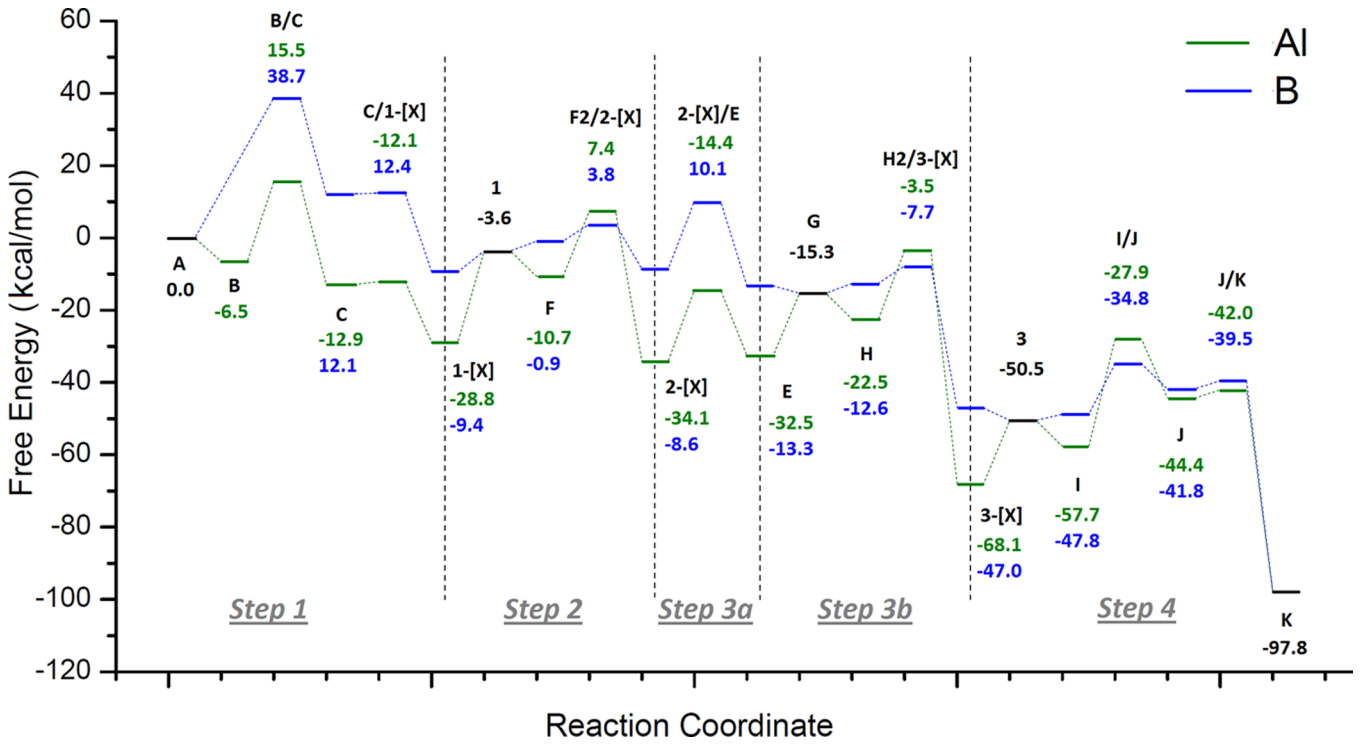

Figure 6. Calculated energy profiles of intermediates and transition states for [B] and [Al] pathways along the reaction coordinate.

[B] seems to be due to the much higher stability of the LA-adducts with [Al] relative to [B], in intermediates **1**-[X], **2**-[X], **E**, and **3**-[X] (see Schemes 5 and 6), which reflects the difficult release of the LA from the substrates and the high barrier for the Si−H bond activation. Focusing on the named intermediates, the relative stability of **1**-[X], **E** and **3**-[X] is more than 10 kcal/mol higher for [Al] than [B], respectively. This result reflects in the key transition states for Si−H activation (i.e., **F2**/**2**-[X] and **H2**/**3**-[X]) lying much higher in energy for [Al]. Moreover, **2**-[X] is favored by −17.1 kcal/mol with [Al] and disfavored by 8.4 kcal/mol with [B] relative to **2**, and **3**-[X] is favored by −17.6 kcal/mol with [Al] and disfavored by 3.5 kcal/mol with [B] with respect to **3** (the total difference between [Al] and [B] is of 25.5 and 21.1 kcal/mol, respectively).

To better understand the large difference in the relative stability of these intermediates, we analyzed both electronic and steric effects. From an electronic point of view, the calculated electrophilicity of the two LAs (0.24 for [Al] and 0.38 for [B]) appears to indicate that the formation of [B]-adducts should be favored relative to the formation of [Al]-adducts. Indeed, the relative energies of the SN_2 H-transfer transition states relative to the preceding intermediates are in line with the electrophilicity results. Moving to sterics, we tested the relative

DOI: 10.1021/jacs.6b01497
J. Am. Chem. Soc. 2016, 138, 5321−5333

stability of **2** and **3** with respect to **2**-[**X**] and **3**-[**X**] with XH_3 (X = Al and B) as LA. The difference in the binding energy of **2** and **3** to AlH_3 and BH_3 is only 2.7 and 4.5 kcal/mol, relative to a difference >20 kcal/mol with [Al] and [B]. Incidentally, the same analysis performed on the LA-$HSiEt_3$ adducts shows that the 10 kcal/mol of difference in the relative stability of the [Al]···H−$SiEt_3$ adduct with respect to the [B]···H−$SiEt_3$ one decreased to −2 kcal/mol in favor of the borane when AlH_3 and BH_3 are used as the LA. This suggests that steric effects strongly impact the binding ability of [B].

As a further test, we decomposed the gas-phase binding energy of [Al] and [B] to formaldehyde into a preparation and an interaction energy term. The first contribution is the energy paid to deform the LA and the aldehyde from their ideal conformations in the unbound state to the geometries they assume in the LA-adducts **E**. The interaction energy term, instead, corresponds to the energy gain due to the rigid interaction between the LA and the aldehyde frozen in the same conformation as in **E**. We found that the deformation of the free [B] to the geometry it has in **E** is 9.5 kcal/mol more expensive than the deformation of [Al], while the interaction energy between the deformed LA and formaldehyde is only 6.5 kcal/mol stronger with [Al]. The two terms cumulate in an [Al]-aldehyde bond being 16.0 kcal/mol stronger than the [B]-aldehyde bond in the gas-phase.

Overall, these results indicated that the different behavior of [Al] and [B] can be ascribed to the significantly smaller size of boron that causes unfavorable steric repulsions between the C_6F_5 rings, as well as between the C_6F_5 rings and the substituents on the silane atoms, in the adducts.

In Scheme 7 we summarized the whole catalytic cycle in the presence of both [Al] and [B] LAs, while the calculated energy profiles of intermediates and transition states for [Al] and [B] pathways along the reaction coordinate were plotted in Figure 6. As the first step, hydrosilylation of CO_2 to silylformate takes place via the [Al] catalyzed C═O activation pathway. Next, the reduction of $HCOOSiEt_3$ to formaldehyde proceeds through the [B] catalyzed SN_2-type Si−H activation mechanism. In the following reduction step to achieve intermediate Et_3SiOCH_3, the C═O and the Si−H activation pathways turn out as competitive with [B] since the corresponding determining barriers are almost the same in energy. Finally, in the last reduction step to methane, the SN_2 Si−H activation mechanism is again favored. The sterics of the substrate seems to play a key role, with the C═O activation pathway suffering the steric hindrance more than the SN_2 Si−H one due to a more crowded geometry of the corresponding transition state.[37] The thermodynamics of the adducts favors [Al]; however, in agreement with the experimental results, only [Al] is active in the first step, while [B] is active in the subsequent steps. As a consequence an exchange between the two Lewis acids is likely to take place during the four reduction steps.

CONCLUSIONS

In summary, we have developed the first example of highly selective reduction of CO_2 into CH_4 via tandem catalytic hydrosilylation by a mixed main-group $B(C_6F_5)_3/Al(C_6F_5)_3$ catalyst system. The results, obtained from our comprehensive study involving the detection, characterization, and independent synthesis of each reaction intermediate, reactions under catalytic conditions, and computational calculations as well as kinetic and mechanistic investigations, have demonstrated that [Al] is responsible for the first step of the reduction that converts CO_2 into $HCOOSiEt_3$, while the subsequent reduction steps of $HCOOSiEt_3$ to $H_2C(OSiEt_3)_2$ to $H_3COSiEt_3$ and finally to CH_4 are catalyzed by [B]. The hydrosilylation of $H_2C(OSiEt_3)_2$, the rate-limiting step in the [B]-catalyzed FLP reduction sequences, is proposed to proceed through a two-step pathway involving the formation and reduction of formaldehyde. Our computational results further address the fixation of CO_2 into $HCOOSiEt_3$ by [Al] via the classical LA-mediated C═O activation, the subsequent transformations into CH_4 by [B] through the FLP-type Si−H activation, as well as the $H_2C(OSiEt_3)_2$ reduction via the formaldehyde cycle, all of which are consistent with the experimental results.

We attribute this remarkably different catalytic behavior between $Al(C_6F_5)_3$ and $B(C_6F_5)_3$ to the higher overall Lewis acidity of [Al] derived from two conflicting factors, electronic and steric effects. While the study of the electronic term indicates that [B] has a higher electronic affinity, the steric term suggests that [B] pays much higher reorganization energy penalty due to both a smaller radius of boron and repulsion between the *ortho*-fluorine atoms. This stronger overall Lewis acidity of [Al], when compared to [B], renders its higher tendency to form stable [Al]−substrate (intermediate) adducts with CO_2 as well as intermediates **1**, **2**, and **3**, hence accounting for its distinct yet complementary catalytic behaviors in the CO_2-to-CH_4 hydrosilylative reduction cycle. Overall, the roles of [Al] and [B] are not only complementary but also synergistic in the total reduction of CO_2, which render both [Al]-mediated first reduction step (which, when carried out alone, is a stoichiometric reaction) and [B]-mediated subsequent steps catalytic. With an optimized loading and [Al]/[B] ratio of 1.0%:5.0%, a high CH_4 production yield of 94% has been achieved. Such a catalytic system is also shown to be recyclable, based on three cycling experiments. The tunability of [Al]/[B] catalysts should allow one to develop more efficient, economical, and recyclable tandem LA catalysts based on inter- or intramolecular and/or heterogeneous catalysts.

ASSOCIATED CONTENT

Supporting Information

The Supporting Information is available free of charge on the ACS Publications website at DOI: 10.1021/jacs.6b01497.

Full experimental details, additional figures, and complete ref 36 (PDF)

Crystallographic data (CIF)

Crystallographic data (CIF)

AUTHOR INFORMATION

Corresponding Authors

*laura.falivene@kaust.edu.sa

*eugene.chen@colostate.edu

Notes

The authors declare no competing financial interest.

ACKNOWLEDGMENTS

This work was supported by the U.S. National Science Foundation (NSF-CHE-1507702) and CSU Energy Institute for the study carried out at Colorado State University and by the funding from King Abdullah University of Science and Technology (KAUST) for the study performed at KAUST. We thank Boulder Scientific Co. for the research gift of $B(C_6F_5)_3$.

DOI: 10.1021/jacs.6b01497
J. Am. Chem. Soc. 2016, 138, 5321−5333

REFERENCES

(1) (a) *Carbon Dioxide as Chemical Feedstock*. Aresta, M., Ed.; Wiley-VCH: Weinheim, 2010. (b) Olah, G. A. *Angew. Chem., Int. Ed.* **2005**, *44*, 2636−2639.

(2) For recent reviews of carbon dioxide conversion and reduction, see: (a) Maeda, C.; Miyazaki, Y.; Ema, T. *Catal. Sci. Technol.* **2014**, *4*, 1482−1497. (b) Oh, Y.; Hu, X. *Chem. Soc. Rev.* **2013**, *42*, 2253−2261. (c) Costentin, C.; Robert, M.; Savéant, J. M. *Chem. Soc. Rev.* **2013**, *42*, 2423−2436. (d) Centi, G.; Quadrelli, E. A.; Perathoner, S. *Energy Environ. Sci.* **2013**, *6*, 1711−1731. (e) Peters, M.; Köhler, B.; Kuckshinrichs, W.; Leitner, W.; Markewitz, P.; Müller, T. E. *ChemSusChem* **2011**, *4*, 1216−1240. (f) Cokoja, M.; Bruckmeier, C.; Rieger, B.; Herrmann, W. A.; Kühn, F. E. *Angew. Chem., Int. Ed.* **2011**, *50*, 8510−37. (g) Riduan, S. N.; Zhang, Y. *Dalton Trans.* **2010**, *39*, 3347−3357. (h) Benson, E. E.; Kubiak, C. P.; Sathrum, A. J.; Smieja, J. M. *Chem. Soc. Rev.* **2009**, *38*, 89−99.

(3) For a recent review of catalytic carbon dioxide hydrosilylation, see: Fernández-Alvarez, F. J.; Aitani, A. M.; Oro, L. A. *Catal. Sci. Technol.* **2014**, *4*, 611−624.

(4) For recent reviews of catalytic carbon dioxide hydrogenation, see: (a) Li, Y.-N.; Ma, R.; He, L.-N.; Diao, Z.-F. *Catal. Sci. Technol.* **2014**, *4*, 1498−1512. (b) Fernández-Alvarez, F. J.; Iglesias, M.; Oro, L. A.; Polo, V. *ChemCatChem* **2013**, *5*, 3481−3494. (c) Wang, W.; Wang, S.; Ma, X.; Gong, J. *Chem. Soc. Rev.* **2011**, *40*, 3703−3727. (d) Federsel, C.; Jackstell, R.; Beller, M. *Angew. Chem., Int. Ed.* **2010**, *49*, 6254−6257. (e) Jessop, P. G.; Joó, F.; Tai, C.-C. *Coord. Chem. Rev.* **2004**, *248*, 2425−2442. (f) Leitner, W. *Angew. Chem., Int. Ed. Engl.* **1995**, *34*, 2207−2221.

(5) (a) Metsanen, T. T.; Oestreich, M. *Organometallics* **2015**, *34*, 543−546. (b) Deglmann, P.; Ember, E.; Hofmann, P.; Pitter, S.; Walter, O. *Chem. - Eur. J.* **2007**, *13*, 2864−2879. (c) Jansen, A.; Görls, H.; Pitter, S. *Organometallics* **2000**, *19*, 135−138. (d) Süss-Fink, G.; Reiner, J. *J. Organomet. Chem.* **1981**, *221*, C36−C38. (e) Koinuma, H.; Kawakami, F.; Kato, H.; Hirai, H. *J. Chem. Soc., Chem. Commun.* **1981**, 213−214.

(6) Scheuermann, M. L.; Semproni, S. P.; Pappas, I.; Chirik, P. J. *Inorg. Chem.* **2014**, *53*, 9463−9465.

(7) Itagaki, S.; Yamaguchi, K.; Mizuno, N. *J. Mol. Catal. A: Chem.* **2013**, *366*, 347−352.

(8) (a) Lalrempuia, R.; Iglesias, M.; Polo, V.; Miguel, P. J. S.; Fernández-Alvarez, F. J.; Peréz-Torrente, J. J.; Oro, L. A. *Angew. Chem., Int. Ed.* **2012**, *51*, 12824−12827. (b) Park, S.; Bézier, D.; Brookhart, M. *J. Am. Chem. Soc.* **2012**, *134*, 11404−11407. (c) Eisenschmid, T. C.; Eisenberg, R. *Organometallics* **1989**, *8*, 1822−1824.

(9) González-Sebastián, L.; Flores-Alamo, M.; García, J. J. *Organometallics* **2013**, *32*, 7186−7194.

(10) (a) Zhang, L.; Cheng, J. H.; Hou, Z. M. *Chem. Commun.* **2013**, *49*, 4782−4784. (b) Motokura, K.; Kashiwame, D.; Takahashi, N.; Miyaji, A.; Baba, T. *Chem. - Eur. J.* **2013**, *19*, 10030−10037. (c) Motokura, K.; Kashiwame, D.; Miyaji, A.; Baba, T. *Org. Lett.* **2012**, *14*, 2642−2645.

(11) Sattler, W.; Parkin, G. *J. Am. Chem. Soc.* **2012**, *134*, 17462−17465.

(12) (a) Piers, W. E. *Adv. Organomet. Chem.* **2004**, *52*, 1−76. (b) Chen, E. Y.-X.; Marks, T. J. *Chem. Rev.* **2000**, *100*, 1391−1434.

(13) Matsuo, T.; Kawaguchi, H. *J. Am. Chem. Soc.* **2006**, *128*, 12362−12363.

(14) Mitton, S. J.; Turculet, L. *Chem. - Eur. J.* **2012**, *18*, 15258−15262.

(15) Jiang, Y. F.; Blacque, O.; Fox, T.; Berke, H. *J. Am. Chem. Soc.* **2013**, *135*, 7751−7760.

(16) (a) LeBlanc, F. A.; Piers, W. E.; Parvez, M. *Angew. Chem., Int. Ed.* **2014**, *53*, 789−792. (b) Berkefeld, A.; Piers, W. E.; Parvez, M.; Castro, L.; Maron, L.; Eisenstein, O. *Chem. Sci.* **2013**, *4*, 2152−2162.

(17) For selected reviews of the FLP chemistry, see: (a) Stephan, D. W.; Erker, G. *Angew. Chem., Int. Ed.* **2015**, *54*, 6400−6441. (b) Stephan, D. W.; Erker, G., Eds.; *Frustrated Lewis Pairs I & II, Topics in Current Chemistry*; Springer-Verlag: Berlin, Germany, 2013; Vols. *332* & *334*. (c) Stephan, D. W.; Erker, G. *Angew. Chem., Int. Ed.* **2010**, *49*, 46−76.

(18) Ashley, A. E.; Thompson, A. L.; O'Hare, D. *Angew. Chem., Int. Ed.* **2009**, *48*, 9839−9843.

(19) Ménard, G.; Stephan, D. W. *J. Am. Chem. Soc.* **2010**, *132*, 1796−1797.

(20) Courtemanche, M.-A.; Légaré, M.-A.; Maron, L.; Fontaine, F.-G. *J. Am. Chem. Soc.* **2013**, *135*, 9326−9329.

(21) For recent reviews of carbon dioxide reduction ultilizing the FLP chemistry, see: (a) Bontemps, S. *Coord. Chem. Rev.* **2016**, *308*, 117−130. (b) Fontaine, F.-G.; Courtemanche, M.-A.; Légaré, M.-A. *Chem. - Eur. J.* **2014**, *20*, 2990−2996.

(22) (a) Declercq, R.; Bouhadir, G.; Bourissou, D.; Légaré, M.-A.; Courtemanche, M.-A.; Nahi, K. S.; Bouchard, N.; Fontaine, F.-G.; Maron, L. *ACS Catal.* **2015**, *5*, 2513−2520. (b) Courtemanche, M.-A.; Pulis, A. P.; Rochette, E.; Légaré, M.-A.; Stephan, D. W.; Fontaine, F.-G. *Chem. Commun.* **2015**, *51*, 9797−9800. (c) Wang, T.; Stephan, D. W. *Chem. - Eur. J.* **2014**, *20*, 3036−3039. (d) Gomes, C. D.; Blondiaux, E.; Thuéry, P.; Cantat, T. *Chem. - Eur. J.* **2014**, *20*, 7098−7106. (e) Courtemanche, M.-A.; Légaré, M.-A.; Maron, L.; Fontaine, F.-G. *J. Am. Chem. Soc.* **2014**, *136*, 10708−10717. (f) Ménard, G.; Stephan, D. W. *Dalton Trans.* **2013**, *42*, 5447−5453. (g) Lim, C. H.; Holder, A. M.; Hynes, J. T.; Musgrave, C. B. *Inorg. Chem.* **2013**, *52*, 10062−10066. (h) Courtemanche, M.-A.; Larouche, J.; Légaré, M.-A.; Bi, W.; Maron, L.; Fontaine, F.-G. *Organometallics* **2013**, *32*, 6804−6811. (i) Roy, L.; Zimmerman, P. M.; Paul, A. *Chem. - Eur. J.* **2011**, *17*, 435−439. (j) Kwon, H. J.; Kim, H. W.; Rhee, Y. M. *Chem. - Eur. J.* **2011**, *17*, 6501−6507. (k) Zimmerman, P. M.; Zhang, Z. Y.; Musgrave, C. B. *Inorg. Chem.* **2010**, *49*, 8724−8728.

(23) Riduan, S. N.; Zhang, Y. G.; Ying, J. Y. *Angew. Chem., Int. Ed.* **2009**, *48*, 3322−3325.

(24) Berkefeld, A.; Piers, W. E.; Parvez, M. *J. Am. Chem. Soc.* **2010**, *132*, 10660−10661.

(25) Schäfer, A.; Saak, W.; Haase, D.; Müller, T. *Angew. Chem., Int. Ed.* **2012**, *51*, 2981−2984.

(26) (a) Wehmschulte, R. J.; Saleh, M.; Powell, D. R. *Organometallics* **2013**, *32*, 6812−6819. (b) Khandelwal, M.; Wehmschulte, R. J. *Angew. Chem., Int. Ed.* **2012**, *51*, 7323−7326.

(27) Chen, E. Y.-X. Tris(pentafluorophenyl)alane. In *Encyclopedia of Reagents for Organic Synthesis*; John Wiley & Sons, Ltd: Hoboken, NJ, 2012, DOI:10.1002/047084289X.rn01382.

(28) (a) Oestreich, M.; Hermeke, J.; Mohr, J. *Chem. Soc. Rev.* **2015**, *44*, 2202−2220. (b) Houghton, A. Y.; Hurmalainen, J.; Mansikkamaki, A.; Piers, W. E.; Tuononen, H. M. *Nat. Chem.* **2014**, *6*, 983−988. (c) Sakata, K.; Fujimoto, H. *J. Org. Chem.* **2013**, *78*, 12505−12512. (d) Piers, W. E.; Marwitz, A. J. V.; Mercier, L. G. *Inorg. Chem.* **2011**, *50*, 12252−12262. (e) Rendler, S.; Oestreich, M. *Angew. Chem., Int. Ed.* **2008**, *47*, 5997−6000. (f) Chojnowski, J.; Rubinsztajn, S.; Cella, J. A.; Fortuniak, W.; Cypryk, M.; Kurjata, J.; Kaźmierski, K. *Organometallics* **2005**, *24*, 6077−6084. (g) Gevorgyan, V.; Rubin, M.; Liu, J.-X.; Yamamoto, Y. *J. Org. Chem.* **2001**, *66*, 1672−1675. (h) Parks, D. J.; Blackwell, J. M.; Piers, W. E. *J. Org. Chem.* **2000**, *65*, 3090−3098. (i) Gevorgyan, V.; Rubin, M.; Benson, S.; Liu, J.-X.; Yamamoto, Y. *J. Org. Chem.* **2000**, *65*, 6179−6186. (j) Parks, D. J.; Piers, W. E. *J. Am. Chem. Soc.* **1996**, *118*, 9440−9441.

(29) To confirm this statement on $B(C_6F_5)_3$ from ref 13, we carried out additional control experiments under our conditions (Table 1, entries 1 and 2). For entry 2, we found no CH_4 formation and only small silane comsuption (~2%), presumably due to the trans-metalation between Et_3SiH and $B(C_6F_5)_3$ in the absence of basic substrates, as reported in: Parks, D. J.; Piers, W. E.; Yap, G. P. A. *Organometallics* **1998**, *17*, 5492−5503.

(30) (a) Chen, J.; Chen, E. Y.-X. *Angew. Chem., Int. Ed.* **2015**, *54*, 6842−6846. (b) Chen, J.; Chen, E. Y.-X. *Molecules* **2015**, *20*, 9575−9590. (c) Timoshkin, A. Y.; Frenking, G. *Organometallics* **2008**, *27*, 371−380. (d) Rodriguez-Delgado, A.; Chen, E. Y.-X. *J. Am. Chem. Soc.* **2005**, *127*, 961−974. (e) Feng, S.; Roof, G. R.; Chen, E. Y.-X. *Organometallics* **2002**, *21*, 832−839. (f) Chen, E. Y.-X.; Kruper, W. J.; Roof, G.; Wilson, D. R. *J. Am. Chem. Soc.* **2001**, *123*, 745−746.

DOI: 10.1021/jacs.6b01497
J. Am. Chem. Soc. 2016, 138, 5321−5333

(31) Chen, J.; Chen, E. Y.-X. *Dalton Trans.* **2016**, *45*, 6105−6110.
(32) Hair, G. S.; Cowley, A. H.; Jones, R. A.; McBurnett, B. G.; Voigt, A. *J. Am. Chem. Soc.* **1999**, *121*, 4922−4923.
(33) Ménard, G.; Gilbert, T. M.; Hatnean, J. A.; Kraft, A.; Krossing, I.; Stephan, D. W. *Organometallics* **2013**, *32*, 4416−4422.
(34) Großekappenberg, H.; Lühmann, N.; Saak, W.; Müller, T. *Z. Anorg. Allg. Chem.* **2015**, *641*, 2543−2548.
(35) Huang, F.; Lu, G.; Zhao, L. L.; Li, H. X.; Wang, Z.-X. *J. Am. Chem. Soc.* **2010**, *132*, 12388−12396.
(36) DFT static calculations were performed using the Gaussian 09 package, see the SI for full computational details.
(37) This result is in agreement with the observations reported in ref 28c for the hydrosilylation of acetone with Me_3SiH and $B(C_6F_5)_3$. In fact, comparing the barrier for the reduction of acetone with that for the reduction of the less hindered formaldehyde, the C═O pathway turns out to be much unfavored for the ketone substrate.

DOI: 10.1021/jacs.6b01497
J. Am. Chem. Soc. 2016, 138, 5321−5333